POLITECNICO DI TORINO
Repository ISTITUZIONALE

Wool-reinforced cement based composites

Original
Wool-reinforced cement based composites / Jozwiak-Niedzwiedzka, D.; Fantilli, A. P.. - In: MATERIALS. - ISSN 1996-1944. - 13:16(2020), pp. 1-13. [10.3390/MA13163590]

Availability:
This version is available at: 11583/2853299 since: 2020-11-19T13:50:13Z

Publisher:
MDPI AG

Published
DOI:10.3390/MA13163590

Terms of use:

This article is made available under terms and conditions as specified in the corresponding bibliographic description in the repository

Publisher copyright

(Article begins on next page)

07 May 2026

A Wideband Highly Linear Distributed Amplifier Using Intermodulation Cancellation Technique for Stacked-HBT Cells

Duy P. Nguyen, *Member, IEEE,* Nguyen L. K. Nguyen, *Student Member, IEEE,* Alexander N. Stameroff, *Member, IEEE,* Vittorio Camarchia, *Senior Member, IEEE,* Marco Pirola, *Member, IEEE,* and Anh-Vu Pham, *Senior Member, IEEE*

***Abstract* — In this paper, a wideband linearization technique for distributed amplifiers is presented. In particular, an auxiliary transistor is employed to create additional intermodulation distortion components that will be feed-forwarded to the output of each gain unit cell to significantly suppress the 3rd order intermodulation distortion (IM3). To verify the concept, two distributed amplifiers (DAs) are fabricated in an Indium Phosphide (InP) process. One amplifier employs a conventional stacked-heterojunction bipolar transistor (HBT) gain unit cell, and the other linearized amplifier utilizes the proposed technique. The linearized distributed amplifier exhibits a measured gain of 10.5 dB with a 3-dB gain bandwidth from dc to 90 GHz. The maximum 1-dB gain compression output power (P_{1dB}) is 20.5 dBm, and the 3rd order intercept point (OIP3) is 33 dBm. Compared to the conventional amplifier, the two values are improved by 3.5 dB and 4.5 dB on average, respectively. Moreover, the linearization technique only increases very little dc power consumption at high power and has the same chip size as compared to the conventional design. To the best of the authors' knowledge, compared to published state-of-the-art DAs, the proposed DA achieves among the highest OIP3 over a wide bandwidth.**

***Index Terms* — Distributed amplifier, feedforward, highly-linear, intermodulation, linearization, InP, MMIC, wideband.**

I. Introduction

As THE demand for high data rate communication systems is increasing rapidly, distributed amplifiers (DAs) are among the critical components to enable such systems, especially for measurement and testing purposes [1]. Typically, the requirements for DAs are high gain and wide bandwidth. However, when the systems become more sophisticated and highly integrated, the amplifiers are also required to have high output power, high linearity, low power consumption, and small chip size. Distributed amplifiers have been presented in various technologies. While Gallium Arsenide (GaAs) and Gallium Nitride (GaN) processes can provide medium to high output power, the gain-bandwidth product (GBW) is limited by their low transition frequencies [2]-[7]. On the other hand, complementary metal-oxide-semiconductor (CMOS) technologies offer wide bandwidth but low output power and poor linearity [8]-[9]. Silicon-on-Insulator (SOI), Silicon Germanium (SiGe), and Indium Phosphide (InP) are among the processes that maintain a good balance between power, bandwidth, and dc consumption [10]-[21].

Different linearization schemes for power amplifiers have been introduced including analog post-distortion [22], pre-distortion [23], active pre-distorter [24], feedforward [25], and harmonic injection [26]-[29]. However, most linearization techniques are inherently narrow-band and only suitable for band-limited amplifiers. Few wideband linearization techniques have been presented to date. [30] presented a CMOS distributed amplifier that uses a distortion cancellation gain unit cell. The technique can achieve up to 5 dB 3rd order intermodulation product (IM3) enhancement, but the bandwidth limits to only 8 GHz. On the other hand, the feedforward linearization concept was extended to linearize a GaAs DA up to 20 GHz [31]. The proposed circuit employed a separated auxiliary amplifier and two phase-shifters, which significantly increases the chip size and limits the bandwidth. Recently, a dc - 65 GHz CMOS DA using active input balun was demonstrated [32]. The amplifier also employs a dual-output two-stage g_m topology to enhance linearity with 10 dBm output power at 1-dB compression (P_{1dB}) reported. However, the linearity enhancement is only achieved at low frequency.

Derivative superposition (DS), which was first presented in [33], [34], is another innovative linearization technique for amplifiers. The technique employs one or more auxiliary transistors to create an external 3rd order intermodulation (IM3) that has an equal amplitude and out-of-phase with the main IM3. Therefore, in theory, the overall 3rd order intermodulation can be canceled. Later, [35] presented a modified DS method using a power series analysis to improve the IIP3 of a low noise amplifier (LNA) while [36], [37] demonstrated a multi-gated transistor technique (MTGR) that was originally based on the Volterra series analysis of the DS technique. Also based on the DS technique, [38] combined both MTGR and capacitance compensation to increase the distributed amplifier linearity from 4 to 8.8 GHz. However, the technique requires the process to have both n-type and p-type transistors. Recently, digitally assisted DS technique has also been presented in [39]. Compared to other conventional linearization methods, the DS technique can provide good IM3 improvement over a wide

This paper is an expanded version from the IEEE MTT-S International Microwave Symposium (IMS2018), Philadelphia, PA, USA, June 10-15, 2018.

Duy P. Nguyen was with University of California, Davis, CA, USA and is currently with MACOM Technology Solutions Inc., Santa Clara, CA, USA. (e-mail: dynguyen@ucdavis.edu)

N. L. K. Nguyen, and A. V. Pham are with the Department of Electrical and Computer Engineering, University of California, Davis, CA, USA (e-mail: nlknguyen@ucdavis.edu; pham@ece.ucdavis.edu).

A. N. Stameroff is currently with Keysight Technologies, Santa Rosa, CA, USA (e-mail: alexander_stameroff@keysight.com).

V. Camarchia and M. Pirola are with the Department of Electronics and telecommunications, Politecnico di Torino, 10129 Turin, Italy (e-mail: vittorio.camarchia@polito.it; marco.pirola@polito.it).

dynamic range while consuming very little extra dc power [40]. However, the DS method has some bandwidth limitations at high frequency. Also, most DS techniques have only been applied for conventional common-source FET topology or cascode FET cells. In addition, the phase and amplitude characteristics over wide bandwidth have not been fully analyzed in previously published works. Hence, high linearity is only achieved in a limited frequency and power range.

A highly linear dc – 90 GHz InP distributed amplifier with the proposed 3rd order intermodulation cancellation technique has been presented in [41]. In the present paper, a detailed mathematical and numerical analysis, simulations, and further experimental results will be reported. The linearization technique proposes a feed-forward IM3 cancellation applied for stacked-Heterojunction Bipolar Transistor (HBT) cells in a distributed amplifier. In particular, the main arm employs a stacked-HBT cell, and an auxiliary arm employs a common-emitter transistor. With a small auxiliary transistor employed, the overall 3rd order intermodulation distortion product is significantly reduced at the output. The 3rd degree coefficient behavior of a stacked-HBT cell is different from that of a single device. Such characteristics will be analyzed in our paper. Secondly, the phase and amplitude characteristics over a wide frequency range are investigated and solutions such as an emitter degeneration resistor and phase-matching transmission lines are proposed to tackle these issues. Finally, linearity responses over temperature, bias variations and the sensitivity of the linearization scheme are demonstrated.

To verify the concept, two millimeter-wave monolithic integrated circuit (MMIC) amplifiers, namely a conventional stacked-HBT DA and a linearized DA are designed, fabricated, and compared using experimental results. Finally, large-signal measurement results up to 85 GHz will be presented to verify the theory and simulation. Both the conventional and linearized DA's exhibit a wide bandwidth of 75 GHz and 90 GHz, with a small-signal gain of 14 dB and 10.5 dB, respectively. Most importantly, the linearized DA achieves a measured maximum output power at 1-dB compression P_{1dB}, saturation power (P_{sat}), and 3rd order intercept point (OIP3) of 20.5 dBm, 22 dBm, and 33 dBm, respectively. As compared to the conventional DA, the results show 3.5 dB, 2 dB, and 4.5 dB improvement in P_{1dB}, P_{sat}, and OIP3, respectively. The linearity enhancement is maintained up to 85 GHz with the same die size and very little increase in dc power consumption. To the best of the author's knowledge, the linearized amplifier achieves the highest bandwidth compared to previous amplifiers using DS method techniques. More importantly, while other DS and MTGR methods only focus on improving the IM3 [40], our proposed DA not only improved the IM3, but it also enhances the 1-dB compression point.

II. Proposed Linearization Technique

A. Harmonic coefficients of an ideal HBT

Fig. 1 shows the simple bias circuit of an HBT transistor. The bias current I_{bias} is fed into the base through a large resistor. The

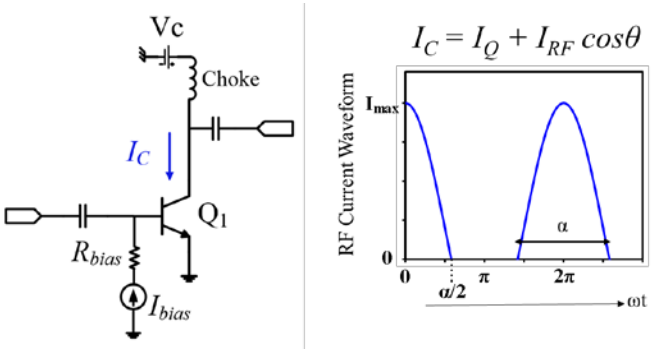

Fig. 1. RF HBT biasing circuit, current waveform, and conduction angle α.

RF input and output are connected through dc blocking capacitors. The conduction angle α is defined as the time interval when the current I_C is positive related to the period (e.g., for class-B bias, $\alpha = \pi$). The conduction angle α is related to the dc collector current, which is controlled by I_{bias}. In general, the RF current at the fundamental frequency depends on the maximum current I_{MAX} and the conduction angle α. In fact, using Fourier transform, the 1st and 3rd degree coefficients a_{i1} and a_{i3} of the collector current can be expressed as (I_1 and I_3 are the fundamental and 3rd harmonic RF current [42]):

$$a_{i1} = \frac{I_1}{I_{MAX}} = \frac{1}{2\pi}\frac{\alpha - sin(\alpha)}{1 - cos(\alpha/2)} \quad (1)$$

$$a_{i3} = \frac{I_3}{I_{MAX}} = \frac{1}{12\pi}\frac{2\,sin(\alpha) - sin(2\alpha)}{1 - cos(\alpha/2)} \quad (2)$$

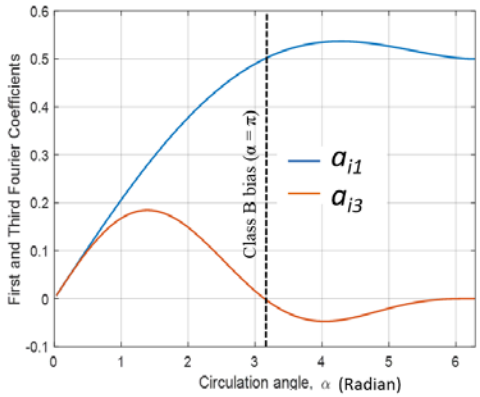

Fig 2. First a_{i1} and third a_{i3} harmonic coefficients as a function of α.

Fig. 2 plots the coefficients a_{i1} and a_{i3} as a function of the conduction angle α in radian, assuming I_{MAX} is constant. It is to be noted that a_{i1} and a_{i3} are the normalized coefficients and dimensionless. It can be seen that while a_{i1} is always positive, the 3rd degree coefficient a_{i3} changes its sign around the class-B bias point, where the conduction angle is 180° (or $\pi \approx 3.14$). Such behavior of the fundamental and 3rd degree coefficients can be used for the amplifier linearization, as first proposed in the derivative superposition method [33], [34]. In this analysis, to effectively exploit this idea, it is necessary to study a_{i1} and a_{i3} behaviors when changing the input power level. It can be proved that the proposed technique can compensate for the 3rd

order intermodulation distortion products over a wide range of output power, not just for a single power level.

To simplify the analysis, we can express the collector current I_C in Fig. 1 with a sinusoidal truncated approximation:

$$I_C = \begin{cases} I_Q + I_{RF}\cos\theta & \text{if } I_Q + I_{RF}\cos\theta > 0 \\ 0 & \text{otherwise} \end{cases} \quad (3)$$

where I_Q represents the equivalent quiescent current, depending on the dc bias. I_Q is the actual quiescent current when it is positive ($I_Q > 0$). When $I_Q < 0$, it becomes a mathematical factor accounting for a conduction angle less than 180 degrees and the actual quiescent current is null. I_{RF} is the RF current modulated by the input voltage and $\theta = \omega t$.

$$I_{RF} = g_m \cdot V_{inp} = g_m \cdot V_{inpMAX}\beta = I_{RFMAX} \cdot \beta \quad (4)$$

$$\beta = \frac{I_{RF}}{I_{RFMAX}} \quad (5)$$

where g_m is the HBT transconductance, and the factor $0 < \beta < 1$ is defined as the ratio between the actual current level I_{RF} with respect to the maximum achievable I_{RFMAX}. Therefore, β is related to the back-off level of the system that represents how far the system operates from the maximum power conditions, where $\beta = 1$. Let us also define the following additional factor:

$$Q = \frac{I_Q}{I_{RFMAX}} \quad (6)$$

In (3), since the current I_C is an even function of θ, only the cosine components will present in the Fourier expansion. Taking the Fourier expansion of (3), for any $n > 0$, we can derive the coefficients a_{in} as shown in (7) – (9). The first three coefficients can be obtained by replacing n = 1, 2, 3 (a_{i1} can be solved by replacing $n = 1$ before taking the integral in (8)):

$$\frac{a_{i1}}{I_{RFMAX}} = \frac{1}{\pi} \cdot Q\frac{\sqrt{\beta^2 - Q^2}}{\beta} + \beta - \frac{\beta}{\pi}\cos^{-1}\left(\frac{Q}{\beta}\right) \quad (10)$$

$$\frac{a_{i2}}{I_{RFMAX}} = \frac{2}{3\pi} \cdot \frac{\beta^2 - Q^2}{\beta^2}\sqrt{\beta^2 - Q^2} \quad (11)$$

$$\frac{a_{i3}}{I_{RFMAX}} = \frac{2}{3\pi} \cdot \frac{Q^2 - \beta^2}{\beta^3} Q\sqrt{\beta^2 - Q^2} \quad (12)$$

The sign and value of Q and β set the operating class of the amplifier. In fact, for $Q > 0$, when $\beta^2 > Q^2$ the amplifier is operating in class AB, while when $\beta^2 < Q^2$ the amplifier is working in class A and expression (10) – (12), that would provide complex values, need to be modified: $a_{i1} = I_{RF}$ and $a_{i2} = a_{i3} = 0$. Instead, for $Q < 0$, when $\beta^2 > Q^2$ the amplifier is working in class C, while for $\beta^2 < Q^2$ the quiescent current is zero (the amplifier is completely off), and all harmonic coefficients a_{in} are null. It is to be noted that the consideration done for the collector current of a single device can be extended to the stacked pair where the two devices share the same collector current.

In the scope of our design, we consider the amplifiers working in the range from class-C up to the lower limit of class-A. Therefore, only the case $\beta^2 \geq Q^2$ is considered when solving for equations, and a_{i1}, a_{i2}, and a_{i3} in (10) – (12) yield real results. From (12), we can see that the 3rd degree coefficient a_{i3} is an odd function of Q, positive when $Q < 0$ (class-C bias) and negative when $Q > 0$ (class-AB bias). More importantly, this feature is independent of β when the transistor operates anywhere from class-C to class-AB. The results here, obtained with a single tone analysis using a piecewise linear transconductance model, will be reused when dealing with the double tone case, considering the intermodulation distortion generation as due to an equivalent power series expansion. Therefore, if the IM3 compensation between the main and auxiliary devices is adjusted for a given power, it will be maintained over a wide range of input power level, ideally up to the maximum operating power ($\beta = 1$).

Based on this analysis, we propose a linearization technique that applies for DA's gain unit cell, in which the main signal path employs a class-AB configuration, and the auxiliary signal path (the linearizer) employs a class-C bias transistor. Since the output voltage of the DA is the in-phase summation of the voltage at each gain unit cell output [1], [43], the overall linearity of the DA is proportional to the linearity of each gain unit cell. In other words, when the IM3 of the gain unit cell is effectively reduced by the proposed technique, the overall IM3 of the DA is also lowered at the same ratio.

B. Proposed wideband linearization technique

Unlike most conventional linearization methods in which the linearization is implemented for a common source FET [33], [34], our proposed distributed amplifier employs a stacked-HBT configuration. Compared to the conventional common-emitter amplifier, the stacked-HBT topology can achieve a higher output power and better bandwidth [11], [44]. Fig. 3(a) presents the stacked-HBT gain unit cell. In the stacked-HBT cell, two transistors Q_1, Q_2 are placed in a common emitter and common base configuration. It is important to note that the resistor-capacitor ($R_b - C_b$) network at the base of Q_1 allows for a certain voltage swing at that node so that the voltage swing will be equally divided between the two transistors [45]-[47]. Therefore, the amplifier can achieve high output power without exceeding the breakdown limit of the process. Moreover, the stacked-HBT structure helps reduce

$$\alpha = 2\cos^{-1}\left(-\frac{I_Q}{I_{RF}}\right) = 2\cos^{-1}\left(-\frac{I_Q}{I_{RFMAX}} \cdot \frac{I_{RFMAX}}{I_{RF}}\right) = 2\cos^{-1}\left(-\frac{Q}{\beta}\right) = 2\left(\pi - \cos^{-1}\left(\frac{Q}{\beta}\right)\right) \quad (7)$$

$$0 \leq \alpha \leq \alpha_{MAX} = \alpha|_{\beta=1} = 2\left(\pi - \cos^{-1}(Q)\right)$$

$$a_{in} = \frac{2}{\pi}\int_0^{\alpha/2}\left(I_Q + I_{RF}\cos\theta\right)\cos(n\theta)\,d\theta = \frac{2}{\pi}I_{RF}\int_0^{\alpha/2}\left(\cos\theta - \cos\frac{\alpha}{2}\right)\cos(n\theta)\,d\theta = \frac{2}{\pi}I_{RFMAX}\beta\int_0^{\alpha/2}\left(\cos\theta - \cos\frac{\alpha}{2}\right)\cos(n\theta)\,d\theta \quad (8)$$

$$\frac{a_{in}}{I_{RFMAX}} = \frac{2}{\pi}(-1)^{n+1} \cdot \frac{n\sqrt{\beta^2 - Q^2}\cos\left(n \cdot \cos^{-1}\left(\frac{Q}{\beta}\right)\right) - Q\sin\left(n \cdot \cos^{-1}\left(\frac{Q}{\beta}\right)\right)}{n(n^2 - 1)} \quad (9)$$

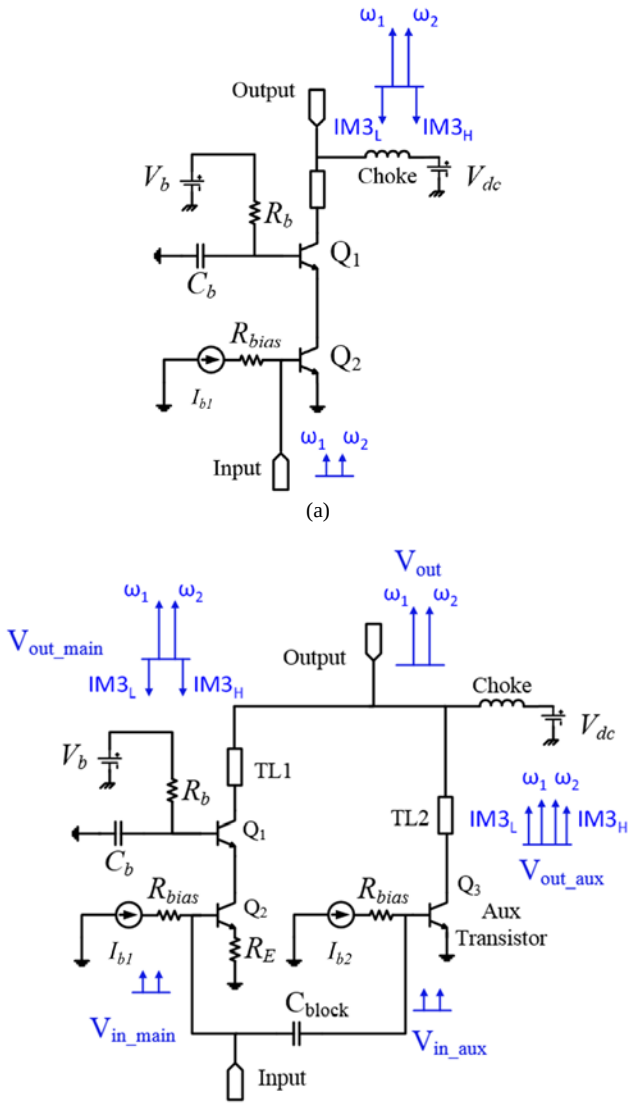

Fig. 3. (a) Conventional stacked-HBT gain unit cell, and (b) proposed linearized gain unit cell.

the Miller effect, resulting in a lower input capacitance. Therefore, a distributed amplifier employing stacked-HBT gain unit cells can achieve higher bandwidth.

Fig. 3(b) illustrates the proposed linearized gain unit cell. The stacked-HBT cell is still the main signal path. An auxiliary small transistor Q_3 is employed and placed in parallel with the main stacked-HBT cell. The main arm and auxiliary arm are biased separately by two current sources I_{b1} and I_{b2}. Besides the device size of the auxiliary transistor Q_3, the bias conditions are critical to achieve the desired linearity. In addition, the main arm employs emitter degeneration resistor R_E to have more control over the phase and amplitude. Finally, the two transmission lines TL1 and TL2 help align the phase of the signals from the main and auxiliary arms to achieve wideband IM3 cancellation. It is worth noting that the main arm employs a stacked-HBT cell to maximize the fundamental output power and bandwidth. On the other hand, the main purpose of the auxiliary arm is to provide negated 3rd order intermodulation product IM3's. Therefore, only a single common-emitter device is used in the auxiliary arm to minimize the overall power consumption. A single auxiliary transistor also reduces the complexity of biasing circuits, layout, and optimization.

To effectively reduce the 3rd order intermodulation products IM3, both the phase and amplitude of the 3rd degree coefficients need to be engineered correctly since all the coefficients are functions of the bias current, input power level, and frequency. If we consider the main stacked-HBT cell as a single-stage amplifier and the input signal has two frequency tones ($\omega_2 > \omega_1$) with equal amplitude, the output voltage (up to 3rd degree) can be expressed as follows:

$$V_{in}(t) = A[\cos(\omega_1 t) + \cos(\omega_2 t)] \tag{13}$$

$$V_{out} = a_1 V_{in} + a_2 V_{in}^2 + a_3 V_{in}^3 \tag{14}$$

where a_1, a_2, a_3 are the first three terms of the power series expansion of the output voltage as a function of the input tone. In particular, a_2 has the unit of V^{-1} and a_3 has the unit of V^{-2}. Although these coefficients are different from a_{i1} and a_{i3} demonstrated in Section II.A, they are related to each other and share similar characteristics. Replacing V_{in} in (14) by (13), the fundamental output voltage V_{out} at frequency ω_1 can be written as [48]:

$$V_{out}(\omega_1 t) = (a_1 A + \tfrac{9}{4} a_3 A^3)\cos(\omega_1 t) \tag{15}$$

In class-AB amplifiers, the value of a_3 has an opposite sign with a_1. Therefore, the term ($a_1A + \frac{9}{4} a_3A^3$) is smaller than a_1A, causing the gain compression in the amplifier. In particular, due to the mixing phenomenon, the high side and low side 3rd order intermodulation products ($IM3_H$ and $IM3_L$), which will appear in the vicinity of ω_1 and ω_2, can be written as [39]:

$$IM3_L = \frac{3}{4} a_3 A^3 \cos[(2\omega_1 - \omega_2)t] \tag{16}$$

$$IM3_H = \frac{3}{4} a_3 A^3 \cos[(2\omega_2 - \omega_1)t] \tag{17}$$

In the proposed design, the auxiliary arm is added to create additional IM3 components. Similarly, (b_1, b_2, b_3) are the fundamental, 2nd degree, and 3rd degree coefficients of the auxiliary device. If the input signal is split between the main and auxiliary arms with a splitting factor γ, then:

$$V_{in_{main}}(t) = \gamma A[\cos(\omega_1 t) + \cos(\omega_2 t)] \tag{18}$$

$$V_{in_{aux}}(t) = (1-\gamma) A[\cos(\omega_1 t) + \cos(\omega_2 t)] \tag{19}$$

$$V_{out}(\omega_1 t) = [a_1\gamma A + \tfrac{9}{4} a_3 \gamma^3 A^3 + b_1(1-\gamma)A + \tfrac{9}{4} b_3 (1-\gamma)^3 A^3]\cos\omega_1 t \tag{20}$$

$$IM3_L = \frac{3}{4} a_3 \gamma^3 A^3 \cos(2\omega_1 - \omega_2)t + \frac{3}{4} b_3 (1-\gamma)^3 A^3 \cos(2\omega_1 - \omega_2)t \tag{21}$$

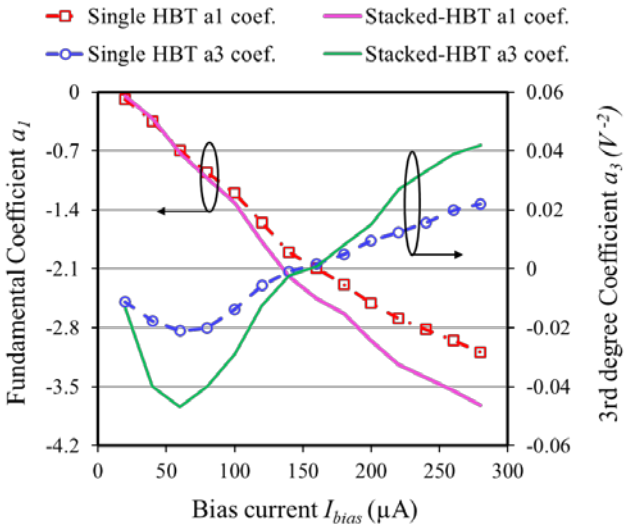

Fig. 4. Fundamental and 3rd degree coefficients of the single common-emitter HBT and stacked-HBT gain unit cell

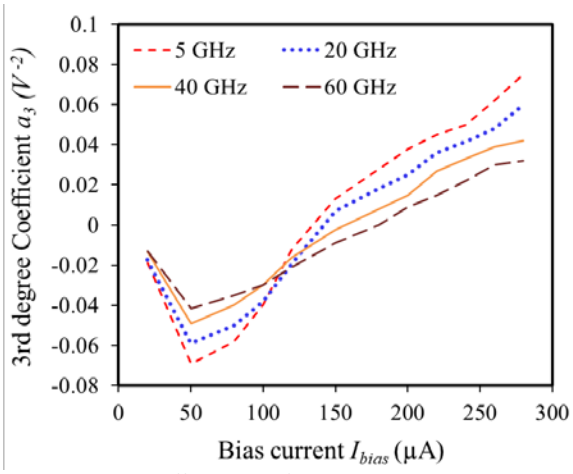

Fig. 5. Third degree coefficient a_3 at frequencies: 5, 20, 40, 60 GHz

The total fundamental signal at ω_1 and the low side IM3 products $IM3_L$ will be expressed in (20) and (21). According to (21), to cancel the IM3 product, the coefficient b_3 need to satisfy the condition:

$$b_3 = -a_3\left(\frac{\gamma}{1-\gamma}\right)^3 \qquad (22)$$

in which the minus sign implies that the auxiliary IM3 has a 180° phase different from the main IM3. In practice, the value of γ depends on the input impedance of the main and auxiliary transistors. Therefore, all the parameters a_3, b_3, and γ in (22) are generally frequency-dependent. Compared to the analysis in previous linearization papers [34]-[37], [39], [40], (22) provides a simple and efficient method for the initial design of the auxiliary transistor to be then further optimized in CAD tools. If we replace b_3 in (20) by (22), the fundamental signal at frequency ω_1 will become:

$$V_{out}(\omega_1 t) = [a_1\gamma A + b_1(1-\gamma)A]\cos\omega_1 t \qquad (23)$$

Identical results can be derived for frequency ω_2 and the high side $IM3_H$; thus are not presented here. With any certain value of a_3 derived from (12) (or extracted from CAD tools), we can engineer an auxiliary arm to have the value of b_3 that satisfies (22), and the overall IM3 signals will be suppressed. Moreover, the value of b_1 is typically smaller than a_1. Therefore, according to (23), the small-signal gain of the linearized amplifier will be smaller than that of the conventional amplifier. The numerical analysis of our proposed linearization method will be discussed in the next section.

III. Linearized Gain Unit Cell

While the previous section presents a theoretical analysis of the proposed technique, simulation using the InP process design kit (PDK) has been conducted to take into account all the effects of frequency-dependent parameters. The degeneration resistor and parasitic emitter inductance create a feedback path from the collector current to the base-emitter voltage. At high frequencies, the feedback path makes the contribution of the 2nd order non-linearity to IM3 become noticeable and eventually limits the IM3 improvement of the proposed technique [35]. In our design, the emitter and the degeneration resistor are connected to the common ground through a co-planar plane to minimize the parasitic inductance. Furthermore, the base bias current is optimized to achieve good linearity improvement at both low and high frequencies.

To extract the coefficient values for our numerical analysis, we simulated both the stacked-HBT and single common-emitter transistor using the components provided in the PDK. The simulation was carried out at different bias currents, temperatures, device peripheries, and frequencies to find the fundamental output V_{out} and 3rd order intermodulation distortion product IM3. Then, the coefficients a_1 and a_3 have been derived using (15) – (17). Since in general, V_{out}, $IM3_L$, and $IM3_H$ have complex values, a_1 and a_3 are also derived in complex terms. In this section, the presentation of the complex a_1 and a_3 is separated into amplitude and phase. Very little difference between the lower side $IM3_L$ and upper side $IM3_H$ is observed in the simulation. The presented a_3 is the average of the two a_3 values calculated from (16) and (17), respectively.

Fig. 4 presents the two coefficients a_1 and a_3 as a function of I_{bias}. The values are extracted from the simulation of a single 10 μm common emitter (CE) HBT device and a stacked-HBT unit cell (both devices in the stack have 10 μm emitter length). It is critical to note that while a_1 is always negative (the negative sign is because of the common-emitter configuration [49]), and its absolute value increases with respect to the bias current, the value of a_3 switches from negative to positive when I_{bias} crosses a certain value (usually around the pinch-off of the HBT device). Moreover, the values of a_1 and a_3 of both single and stacked configurations change in the same manner. However, the stacked-HBT has a higher fundamental gain as well as higher 3rd degree coefficients. Therefore, to linearize a stacked-HBT cell, the auxiliary arm needs to supply a higher IM3 amplitude.

The behavior of the 3rd degree coefficient a_3 is further investigated over different frequencies and different temperatures. Fig. 5 shows the simulated coefficient a_3 of the stacked-HBT cell at four different frequencies across the band:

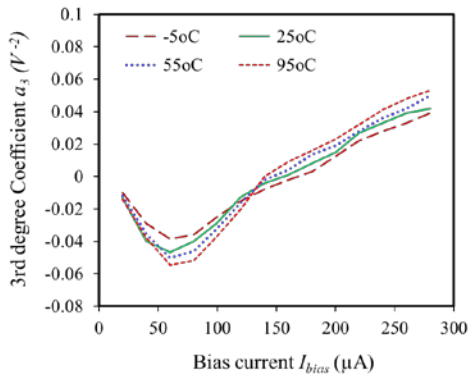

Fig. 6. Third degree coefficient a_3 at temperature: -5, 25, 55, 95ºC.

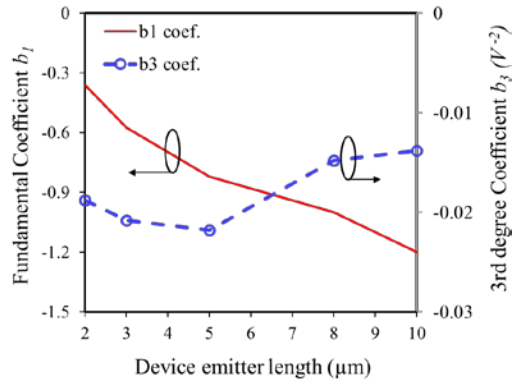

Fig. 7. Fundamental and 3rd degree coefficients of the auxiliary device Q_3 at I_{bias} = 100 μA.

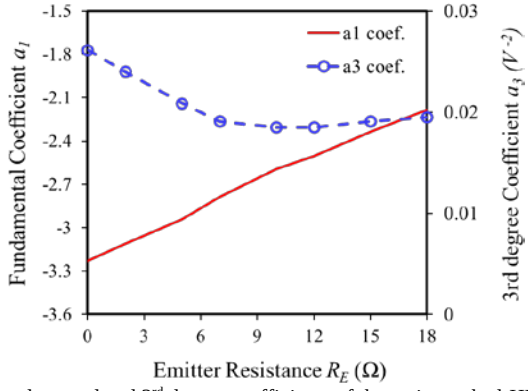

Fig. 8. Fundamental and 3rd degree coefficients of the main stacked-HBT cell with emitter degeneration R_E.

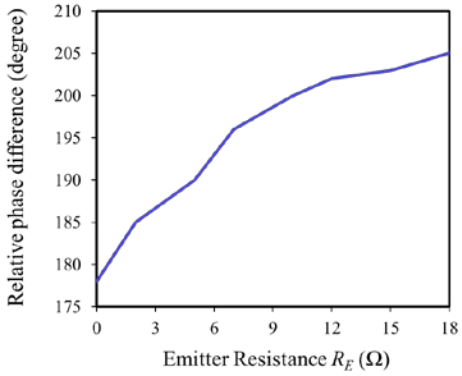

Fig. 9. Simulated relative phase difference between the fundamental and 3rd IM3 with emitter degeneration R_E.

5, 20, 40, and 60 GHz. Although the absolute values of a_3 vary over frequencies, the sign flipping behavior still maintains across the frequency band of interest. More importantly, at the frequencies where a_3 has a higher absolute positive value (e.g., 5 GHz), it also has a higher absolute negative value. This phenomenon helps maintain the linearization over a very wide bandwidth. Fig. 6 presents the a_3 coefficient over temperature from -5ºC to 95ºC. The variation of a_3 over temperature shares a similar trend but is much smaller than the variation over frequency. It is also worth noting that the "switching points" (where a_3 changes from negative to positive) are different at different frequencies and temperatures.

From the above analysis, since the main stacked-HBT cell is biased in class-AB, a_3 will be positive. Therefore, if we bias the auxiliary device below the "switching point", we can have a negative b_3. Hence, the two IM3 signals from the main and auxiliary arms will be 180º phase different. Besides the 180º phase different requirement, to suppress the IM3 products, the amplitudes of a_3 and b_3 also need to satisfy (22). The critical parameter that determines the value of b_3 is the emitter length of the auxiliary device. The device size is not only chosen to achieve the required b_3, but also to minimize the dc power consumption. Typically, the smaller the device, the less dc power dissipation. Fig. 7 shows the b_1 and b_3 coefficients of different device sizes at I_{bias} = 100 μA. Regarding the absolute values, while b_1 increases as the device become larger, b_3 only maintains high absolute values when the device is small. In our proposed design, we choose the auxiliary HBT emitter length to be 5 μm to have the b_3 = -0.022 V^{-2}.

In addition to choosing the auxiliary device size and its dc bias condition, the main signal path can also be optimized to further linearize the gain unit cell. In [50], two degenerated resistors are introduced in both the main and auxiliary arms to optimize just for the amplitude matching. In our proposed design, only in the main arm, an emitter degeneration resistor will be added to modify both the amplitude and phase characteristics of the signal. Fig. 8 and Fig. 9 present the simulated amplitude and phase of the stacked-HBT cell (emitter length 10 μm) at I_{bias} = 220 μA with an emitter degeneration resistor R_E. With R_E = 5 Ω, the value of a_3 can be reduced to match with b_3. Moreover, with R_E added, the phase can be changed and optimized for phase alignment between the main IM3 and auxiliary IM3 to achieve highest IM3 cancellation over a wide bandwidth. Although adding R_E reduces the overall amplifier gain, it helps achieving a better alignment for both the IM3 phase and amplitude between the main and auxiliary arms, therefore ensuring that the here proposed linearization technique can perform well over a wide frequency range.

IV. Distributed Amplifier Design

To verify the proposed concept, two distributed amplifiers are designed and fabricated. The schematic diagrams of the amplifiers are shown in Fig. 10. For the conventional DA, the gain unit cell is the one in Fig. 3(a) and for the linearized DA, the unit cell is shown in Fig. 3(b). For the linearized DA, an additional bias current I_{b2} is required. The amplifier employs

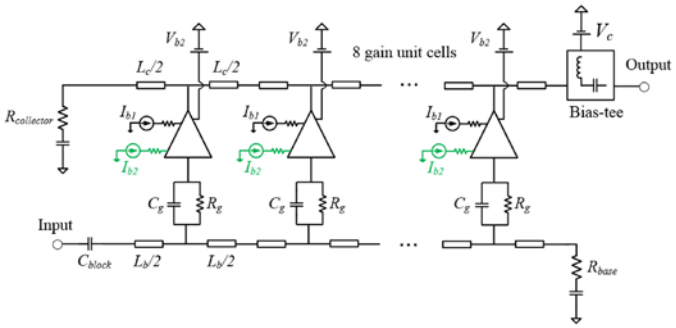

Fig. 10. Schematic diagram of the proposed distributed amplifier.

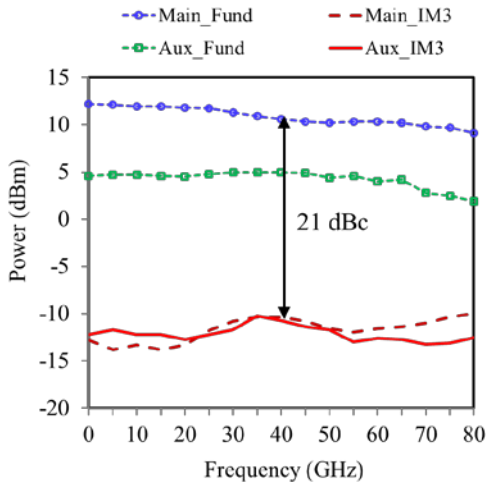

(a)

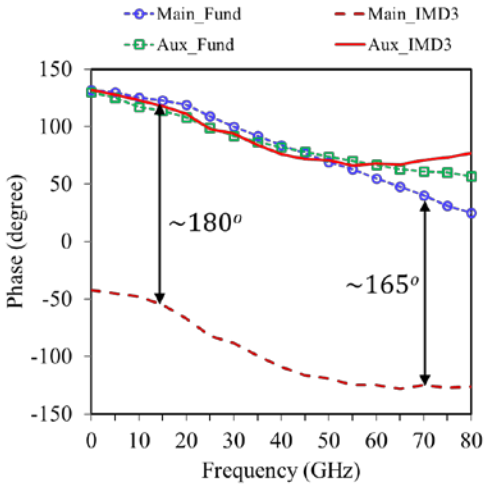

(b)

Fig. 11. Simulated amplitude (a) and phase (b) of the fundamental components and 3rd order intermodulation products at the output of the main and auxiliary paths under two-tone excitation.

eight identical gain unit cells. At the input of each gain unit cell, a parallel RC network is added to reduce the overall input capacitance and extend the DA bandwidth up to 90 GHz [11]. The base and collector transmission lines, as well as termination resistors R_{base} and $R_{collector}$ are designed to achieve wideband input and output matching. Since the gain unit cells of the two amplifiers are different, the design parameters of the two DAs are also different and are presented in Table I.

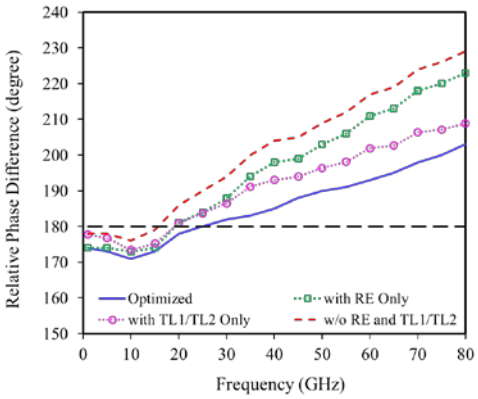

Fig. 12. Relative phase difference between the main IM3 and auxiliary IM3 signals versus frequency under the impact of TL1/TL2 and R_E.

TABLE I
DESIGN PARAMETERS OF THE TWO AMPLIFIERS

Design parameters		Conventional DA	Linearized DA
Gain unit cell	Topology	Stacked-HBT	Linearized cell
	R_E	0 Ω	5 Ω
Bias conditions	I_{b1}	220 μA	220 μA
	I_{b2}	N/A	100 μA
	V_c	4 V	4 V
	V_{b2}	1.8 V	1.8 V
Input RC network	C_g	90 fF	75 fF
	R_g	1000 Ω	1000 Ω
Inductances	L_b	36 pH	24 pH
	L_c	90 pH	66 pH
Terminations	R_{base}	50 Ω	50 Ω
	$R_{collector}$	50 Ω	47 Ω

The simulation of the linearized DA shown in Fig. 10 was carried out using Keysight Advanced Design System (ADS) to verify the proposed design. The simulation of the full amplifier with eight gain unit cells took into consideration of all the loading effects and parasitics. Current and voltage probes are placed at the output of the main and auxiliary arms to measure the power contributed by each arm separately.

Fig. 11 presents the simulated amplitude and phase of the main and auxiliary arms with the input power of the gain unit cell at 0 dBm, which is close to the 1-dB compression point of the main stacked-HBT cell. The fundamental component of the auxiliary path is smaller than that of the main path since it is a smaller transistor. However, the auxiliary device is biased with a lower current and can generate similar IM3 products. Therefore, the IM3 signals of the two arms have equal amplitude. Besides the amplitude, the phase characteristic of the two signals is also critical for linearizing the amplifier. As shown in Fig. 11(b), the phases of the fundamental component and IM3 component of the main path are 180° different. On the other hand, the auxiliary path generates the fundamental signal and IM3 signal that are in-phase with each other. As a result, the IM3 signals of the two arms have the same amplitude and

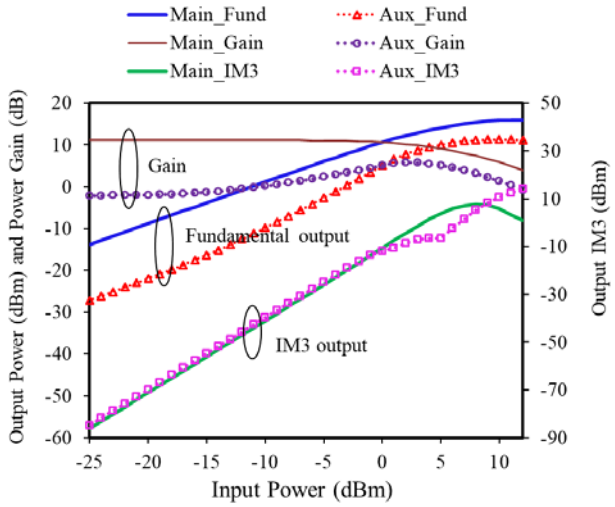

Fig. 13. Fundamental and IM3 amplitude as a function of input power at 40 GHz.

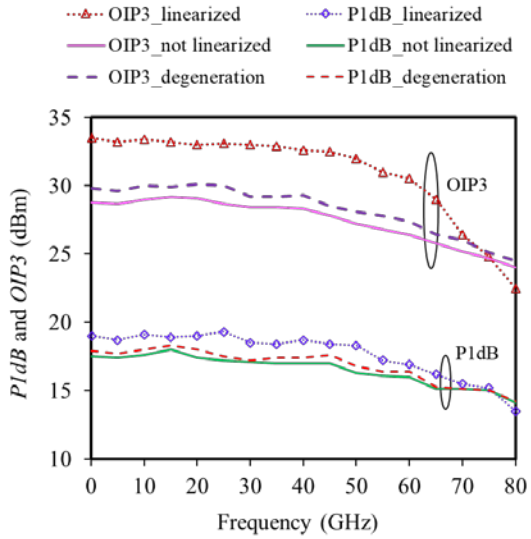

Fig. 14. Simulated P_{1dB} and OIP3 of the linearized DA and conventional DA over frequency.

180° out of phase. Ideally, they will cancel and provide a significant improvement in linearity. In practice, the amplitude and phase characteristics of the auxiliary transistor start to deviate from the designed values at frequencies larger than 65 GHz. For instance, at low frequencies, the relative phase difference between the fundamental signal and IM3 signal of the main arm is well aligned with the theory, which is about 180°. However, at high frequencies, that phase difference reduces to around 165°. The phase variations in both the main and auxiliary arms make the IM3 cancellation less effective at high frequencies. Hence, two transmission lines TL1 and TL2 along with an emitter degeneration resistor R_E are added to further optimize the phase alignment.

Fig. 12 demonstrates the relative phase offset between the main and auxiliary IM3 signals in different cases: without R_E and TL1/TL2, with each of the component separately, and the fully optimized design (include both R_E and TL1/TL2). Ideally, this phase offset needs to be close to 180° to achieve good IM3 cancellation. The original phase offset without R_E and the two transmission lines deviates far from 180° starting from 30 GHz. The TL1 and TL2 are 200 µm different in physical length. Assuming the physical length is fixed, the electrical length increases proportionally with respect to the frequency. At low frequencies, the 200 µm long transmission line results in very little change in electrical length between the two paths, but it causes a significant phase difference at high frequencies. Such an interesting characteristic along with the phase changes provided by the degenerated resistor R_E help bring the phase offset much closer to 180° across the whole frequency band.

Fig. 13 presents the simulated fundamental, power gain, and IM3 amplitude of the main arm and auxiliary arm at 40 GHz as a function of input power. All the device size, bias condition, and phase alignment are designed to perfectly match the IM3 amplitude of both arms. The fundamental signal of the auxiliary arm experiences a gain expansion and starts to compress earlier than the main signal. The linearization technique performs well over a wide dynamic range of input power from below -25 dBm up to -3 dBm. As the transistors compress, the IM3 starts to have a dip at a certain power level [51]. However, the technique can still provide excellent linearity enhancement up to 1-dB gain compression point. Simulated P_{1dB} and OIP3 comparison between a conventional DA, a conventional DA with resistive degeneration, and the linearized DA are presented in Fig. 14. While the degenerated resistor alone only provides very little linearity enhancement, the proposed linearization technique observes a significant improvement. Compared to the conventional DA, the linearized DA has an average of 1.4 dB higher in the 1-dB compression point P_{1dB} and 4.2 dB higher in the 3rd order intercept point OIP3. The linearity enhancement achieves the best performance from dc to 65 GHz, corresponding to the frequency range where perfect phase alignment is achieved in Fig. 11(b).

V. Experimental Results

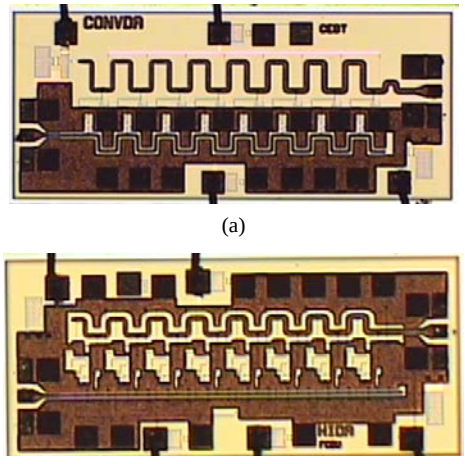

(a)

(b)

Fig. 15. Chip photograph of (a) conventional stacked-HBT DA, and (b) proposed linearized DA.

The two distributed amplifiers are designed and fabricated in an InP HBT process. The process has a transition frequency f_T of 250 GHz and a maximum frequency f_{max} of 380 GHz. The

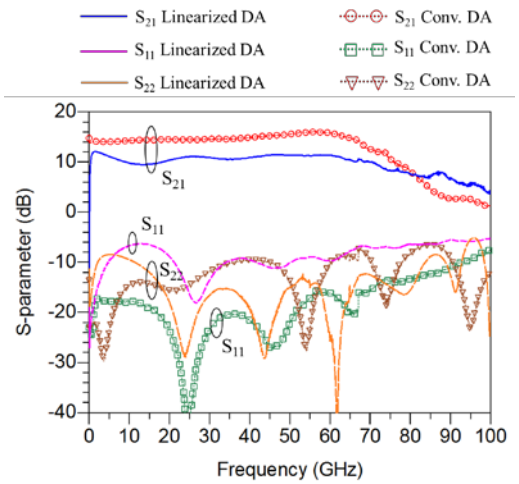

Fig. 16. Measured S-parameter of the conventional DA and proposed linearized DA.

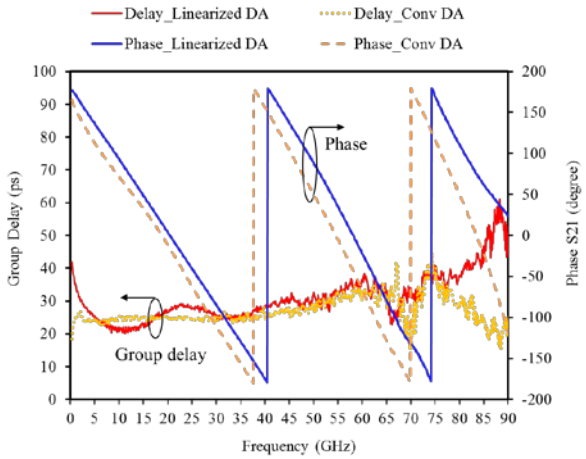

Fig. 17. Measured phase and group delay

chip photos are shown in Fig. 15. All the input and output inductances are realized by coplanar transmission lines except the output inductance of the conventional DA uses microstrip lines. The current sources I_{b1} and I_{b2} are provided by two bond pads. Wideband terminations at both the base and collector are designed using several RC networks placed in parallel, including a bond pad that connects to a 10 µF off-chip capacitor. Both DAs have the die area of 1.6 x 0.7 mm^2 including all pads. The proposed linearization technique does not increase the chip size. All the measured results are based on the bias condition depicted in Table I. At small signal condition, both amplifiers draw around 100 mA collector current. In the proposed linearized DA, the collector current increases to 150 mA when the amplifier reaches maximum output power.

Fig. 16 illustrates the measured frequency responses of the two DAs. The conventional amplifier has a small signal gain of 14 dB, and the 3-dB gain bandwidth of 75 GHz. The proposed linearized amplifier exhibits an average gain of 10.5 dB. The 3-dB gain bandwidth covers up to 90 GHz, making the gain-bandwidth product of 301 GHz. Compared to the conventional DA, the linearized DA has 3.5 dB lower small-signal gain since the input signal is split into the main arm and auxiliary arm by a factor of γ. However, while the gain of the conventional DA

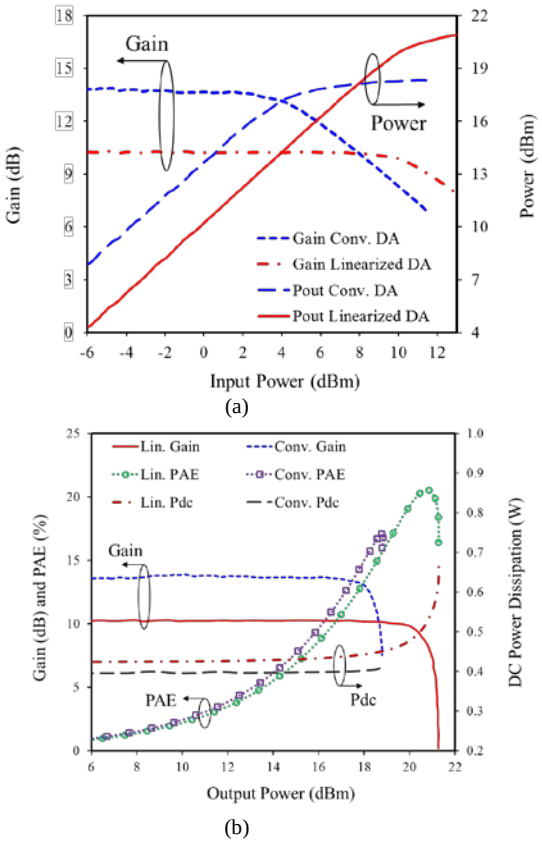

Fig. 18. (a) Measured output power and gain at continuous wave (CW) 20 GHz, and (b) dc power dissipation and PAE versus output power of the conventional DA and proposed linearized DA.

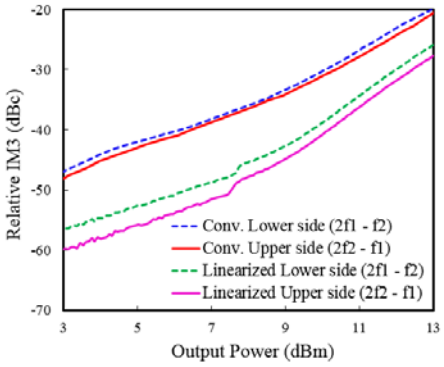

Fig. 19. Measured relative IM3 components of the conventional DA and linearized DA at 20 GHz using two-tone excitation with 10 MHz tone spacing.

rolls off quickly beyond 75 GHz, the linearized DA can extend the bandwidth up to 90 GHz. Both amplifiers have good input and output return losses over the entire frequency band. Fig. 17 presents the measured insertion phase and group delay of the two distributed amplifiers. The two amplifiers exhibit a similar phase and group delay performance up to 65 GHz. Although the conventional DA has a flatter in-band group delay, when the frequency goes above 65 GHz, its group delay starts to deviate and change more abruptly since it has a much stepper gain slope and lower bandwidth than the linearized DA.

Fig. 18(a) presents the measured large signal output power and gain of the linearized and conventional amplifiers at

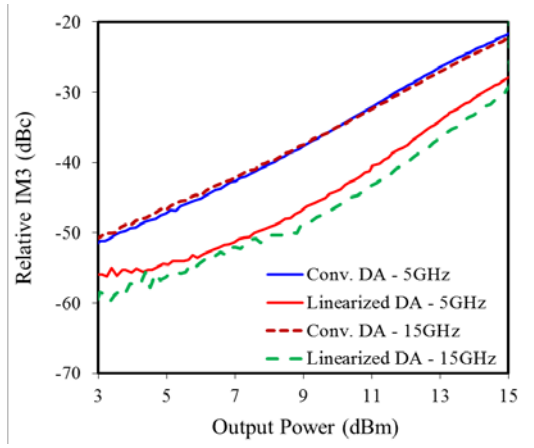

(a)

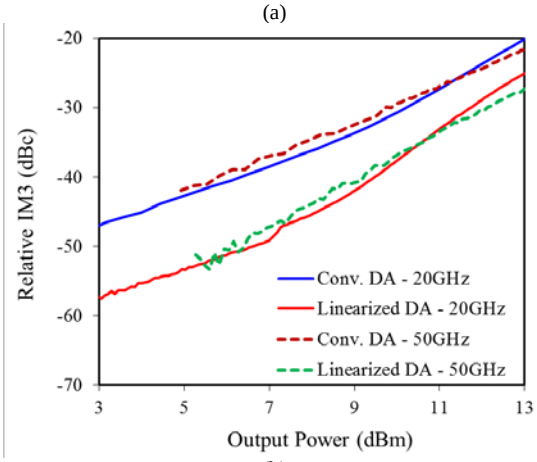

(b)

Fig. 20. Measured relative IM3 using two-tone excitation with 10 MHz tone spacing of the conventional DA and proposed linearized DA: (a) center frequency 5 GHz and 15 GHz, and (b) center frequency 20 GHz and 50 GHz.

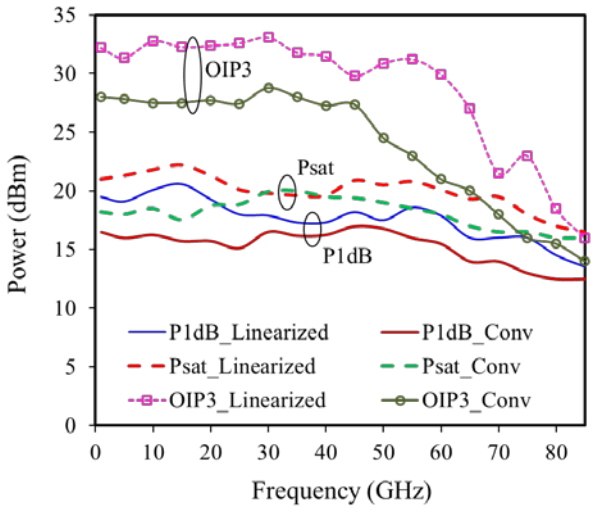

Fig. 21. Measured P_{1dB}, P_{sat}, and *OIP3* as a function of frequency (at room temperature, nominal condition).

20 GHz. Although having 3.5 dB less gain than the conventional design, the proposed linearized amplifier achieves 3 dB higher P_{1dB} and 2.5 dB higher P_{sat}, significantly extend the linear operation region of the amplifier. Fig. 18(b) further illustrates the total dc power dissipation and power added efficiency (PAE) of the two amplifiers. At low power, the linearized DA consumes 20 mW more than the conventional amplifier does, and the total dc current rises up to 150 mA at 21 dBm output power. Both amplifiers reach peak PAE at around its P_{1dB} compression point. Since the linearized DA can achieve higher output power, its peak PAE is 3% higher than the conventional DA despite consuming more dc power. Fig. 19 demonstrates the relative IM3 components from a two-tone measurement of the two distributed amplifiers at the center frequency of 20 GHz and a tone spacing of 10 MHz. The lower side IM3 component, which is the spectrum at frequency $2f_1 - f_2$, is improved by 10 dB in the low power region and by 6 dB at high output power. Similarly, the upper side IM3 component ($2f_2 - f_1$) is improved by 13 dB in the low power and 7 dB at high power. In both DAs, the lower side IM3 component is always higher than the upper side IM3 component.

Since the linearized amplifier has 3-dB gain lower than the conventional amplifier, the IM3 of the two amplifiers should be measured at the same output power level to provide a fair comparison. Fig. 20 shows the relative IM3's of the two amplifiers as a function of output power under two-tone excitation centered at different frequencies across the band with a tone spacing of 10 MHz. To simplify the plots, all the IM3 components shown in Fig. 20 are the average of the lower side and upper side IM3 components. The average IM3 value is also used for OIP3 calculation. The linearized DA shows an average of 10 dB IM3 improvement, with the maximum improvement of 12 dB is observed at 20 GHz. The IM3 is also significantly suppressed from low output power region up to high output power. Most importantly, unlike other conventional linearization techniques having limited bandwidth, the proposed linearization scheme exhibits consistent performance over a very wide frequency range.

Fig. 21 illustrates the measured power and linearity of the two DAs from 1 to 85 GHz. In the proposed linearized DA, the maximum P_{1dB} is 20.5 dBm, and the highest P_{sat} is 22 dBm, which is 3.5 dB and 2 dB improvement, respectively. As compared to the conventional DA. The measured maximum *OIP3* is 33 dBm achieved from 1 to 30 GHz, showing excellent linearity performance. From dc to 85 GHz, on average, P_{1dB} and P_{sat} are improved by 1.5 dB and 2.5 dB, respectively. The P_{1dB} and P_{sat} also show flat response and only slightly rolls off beyond 65 GHz. Most importantly, big enhancements in *OIP3* are observed from dc to 65 GHz, with 5 dB improvement at low frequencies and up to 7 dB improvement at high frequencies. The *OIP3* of both DAs roll-off at high frequency, but the linearized DA still shows higher *OIP3* relative to the conventional design. Fig. 22 presents the measured versus simulated P_{1dB} and *OIP3* of the linearized amplifier. The measured results are well correlated with simulation over the entire frequency band except for faster roll-off in *OIP3* beyond 65 GHz. The sensitivity of the proposed linearization method over temperature and bias variations is demonstrated in Fig. 23. According to the measured results shown in Fig. 23(a), the OIP3 is slightly decreased when the temperature increases with an average 0.9 dB lower at 55°C and 1.9 dB lower at 95°C.

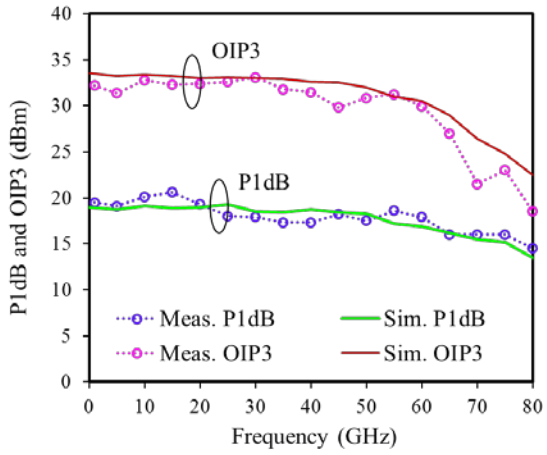

Fig. 22. Measured versus simulated P_{1dB} and *OIP3* of the proposed linearized DA.

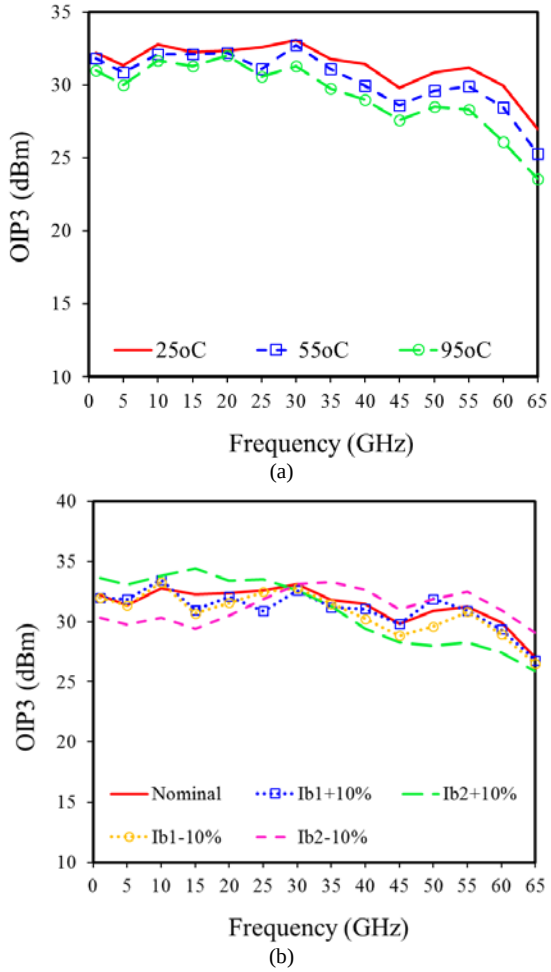

Fig. 23. Measured *OIP3* of the linearized DA at (a) different backside temperature and (b) different bias variants.

Fig. 23(b) presents the *OIP3* when the bias current of the main arm (I_{b1}) is varied by ±10% and the bias current of the auxiliary arm (I_{b2}) is varied by ±10% (when I_{b1} is varied, I_{b2} is kept constant and vice versa). While *OIP3* is insensitive to I_{b1} changes, the changes in I_{b2} affect the *OIP3* response over frequency. When I_{b2} increases, the linearity is better at low frequencies and worse at high frequencies due to the shift in the phase and amplitude match curves. The effect is reversed when I_{b2} decreases. At the nominal condition, the bias currents are optimized to achieve flat *OIP3* over the entire bandwidth.

The proposed linearized DA presents a significant enhancement in power and linearity with a trade-off in small-signal gain and little increase in dc power consumption. To provide a fair comparison, we define the figure of merit (FOM) including all critical specifications of an amplifier as followed:

$$\text{FOM} = \frac{\text{Gain} \cdot \text{Bandwidth} \cdot OIP3}{P_{dc}}$$

in which gain is in linear scale, *OIP3* and P_{dc} are in Watt. Performance summary of state-of-the-art wideband distributed amplifiers published in the literature as well as of our prototype is presented in Table II. It can be seen that the *OIP3*/P_{dc} ratio is typically highest in GaN technologies, follow by GaAs and InP, and the lowest is Silicon-based technologies.

TABLE II
COMPARISON TO OTHER STATE-OF-THE-ART DAS

Ref	Gain (dB)	BW (GHz)	P_{sat} (dBm)	*OIP3* (dBm)	P_{dc} (W)	*OIP3*/ P_{dc}	FOM	Tech.
[2]	12	dc-22	30.8	41	2.5	5	441	GaAs
[3]	10	0.1 - 45	30-33	28-41	5.2	2.4	345	GaN
[4]	13	1-25	20	33.5	0.9	2.5	267	GaN
[7]	12	0.1 - 8	35	48	4.4	11.4	363	GaN
[8]	7	dc - 61	NA	10.9	0.06	0.2	28	CMOS
[9]	7	dc - 70	10	16.3	0.12	0.4	56	CMOS
[10]	7.8	4 - 86	11	15.5	0.13	0.3	55	SOI
[11]	16	1.5 - 88	19.5	27.5	0.48	1.2	636	InP
[12]	11	dc - 90	12	15.5	0.21	0.2	54	SOI
[32]	22	dc - 65	10	NA	0.1	NA	NA	CMOS
[52]	8.6	2 - 41	7.8	16.8	0.02	2.4	251	CMOS
[53]	14	dc – 73	3.2	NR	0.084	NA	NA	CMOS
Conv. DA	**14**	**dc - 75**	**20**	**28**	**0.4**	**1.6**	**593**	**InP**
Lin. DA	**10.5**	**dc - 90**	**22**	**33**	**0.4**	**5**	**1504**	**InP**

VI. CONCLUSION

A wideband linearization technique for stacked-HBT distributed amplifiers has been introduced and analyzed. The proposed concept is then experimentally illustrated in a dc – 90 GHz InP distributed amplifier. Compared to the conventional approach, the linearized DA exhibits significant linearity enhancement over a very wide bandwidth up to 85 GHz. The amplifier has a measured maximum P_{1dB} of 20.5 dBm, and highest OIP3 of 33 dBm. The OIP3 is improved by more than 5 dB from dc to 65 GHz. Moreover, the power and linearity enhancement is achieved with only a trade-off in small-signal gain and little increase in dc power dissipation.

ACKNOWLEDGMENT

We appreciate the support of Keysight Technologies under the Core Technology University Research program.

REFERENCES

[1] J. B. Beyer, S. N. Prasad, R. C. Becker, J. E. Nordman, and G. K. Hohenwarter, "MESFET Distributed Amplifier Design Guidelines," *IEEE Trans. Microw. Theory Techn.*, vol. 32, no. 3, pp. 268-275, 1984.

[2] K. Fujii, "A DC to 22GHz, 2W high power distributed amplifier using stacked FET topology with gate periphery tapering," in *Proc. IEEE Radio Freq. Integr. Circuits Symp. (RFIC)*, 2016, pp. 270-273.

[3] K. W. Kobayashi, D. Denninghoff, and D. Miller, "A Novel 100 MHz-45 GHz Input-Termination-Less Distributed Amplifier Design With Low-Frequency Low-Noise and High Linearity Implemented With A 6 Inch GaN-SiC Wafer Process Technology," *IEEE J. Solid-State Circuits*, vol. 51, no. 9, pp. 2017-2026, 2016.

[4] M. Chen *et al.*, "A 1-25 GHz GaN HEMT MMIC Low-Noise Amplifier," *IEEE Microw. Wireless Compon. Lett.*, vol. 20, no. 10, pp. 563-565, 2010.

[5] C. Campbell *et al.*, "A Wideband Power Amplifier MMIC Utilizing GaN on SiC HEMT Technology," *IEEE J. Solid-State Circuits*, vol. 44, no. 10, pp. 2640-2647, 2009.

[6] G. Nikandish and A. Medi, "Unilateralization of MMIC Distributed Amplifiers," *IEEE Trans. Microw. Theory Techn.*, vol. 62, no. 12, pp. 3041-3052, 2014.

[7] J. Moon *et al.*, "100 MHz–8 GHz linear distributed GaN MMIC power amplifier with improved power-added efficiency," in *Proc. IEEE Topical Conf. RF/Microw. Power Amplif. Radio Wireless Appl. (PAWR)*, Jan. 2017, pp. 40-43.

[8] C. Y. Hsiao, T. Y. Su, and S. S. H. Hsu, "CMOS Distributed Amplifiers Using Gate-Drain Transformer Feedback Technique," *IEEE Trans. Microw. Theory Techn.*, vol. 61, no. 8, pp. 2901-2910, 2013.

[9] T. Ming-Da, W. Huei, K. Jui-Feng, and C. Chih-Sheng, "A 70GHz cascaded multi-stage distributed amplifier in 90nm CMOS technology," in *IEEE Int. Solid-State Circuits Conf. (ISSCC) Dig. Tech. Papers*, 2005, pp. 402-606.

[10] J. O. Plouchart *et al.*, "A 4-91 GHz traveling-wave amplifier in a standard 0.12um SOI CMOS microprocessor technology," *IEEE J. Solid-State Circuits*, vol. 39, no. 9, pp. 1455-1461, 2004.

[11] D. P. Nguyen, A. N. Stameroff, and A. V. Pham, "A 1.5-88 GHz 19.5 dBm output power triple stacked HBT InP distributed amplifier," in *IEEE MTT-S Int. Microw. Symp. Dig. (IMS)*, 2017, pp. 20-23.

[12] K. Jonghae *et al.*, "A 12dBm 320GHz GBW distributed amplifier in a 0.12um SOI CMOS," in *IEEE Int. Solid-State Circuits Conf. (ISSCC) Dig. Tech. Papers*, 2004, pp. 478-540.

[13] E. Cohen *et al.*, "75 GHz InP HBT distributed amplifier with record figures of merit and low power dissipation," *IEEE Trans. on Electron Devices*, vol. 53, no. 2, pp. 392-394, 2006.

[14] P. Rito, I. G. Líópez, A. Awny, A. C. Ulusoy, and D. Kissinger, "A DC-90 GHz 4-Vpp differential linear driver in a 0.13 um SiGe BiCMOS technology for optical modulators," in *IEEE MTT-S Int. Microw. Symp. Dig. (IMS)*, 2017, pp. 439-442.

[15] O. Wohlgemuth, P. Paschke, and Y. Baeyens, "SiGe broadband amplifiers with up to 80 GHz bandwidth for optical applications at 43 Gbit/s and beyond," in *33rd European Microw. Conf. (EuMC)*, 2003, pp. 1087-1090.

[16] S. Handa *et al.*, "60 GHz-band low noise amplifier and power amplifier using InGaP/GaAs HBT technology," in *IEEE Gallium Arsenide Integr. Circuit (GaAs IC) Symp. Dig.*, 2003, pp. 227-230.

[17] K. Nishikawa, T. Enoki, S. Sugitani, and I. Toyoda, "0.4 V, 5.6 mW InP HEMT V-band Low-Noise Amplifier MMIC," in *IEEE MTT-S Int. Microw. Symp. Dig. (IMS)*, 2006, pp. 810-813.

[18] K. Elgaid, H. McLelland, C. R. Stariley, and I. G. Thayne, "Low noise W-band MMMIC amplifier using 50nm InP technology for millimeterwave receivers applications," in *Int. Conf. Indium Phosphide and Related Materials*, 2005, pp. 523-525.

[19] S. Masuda, T. Ohki, and T. Hirose, "Very Compact High-Gain Broadband Low-Noise Amplifier in InP HEMT Technology," *IEEE Trans. Microw. Theory Techn.*, vol. 54, no. 12, pp. 4565-4571, 2006.

[20] J. B. Hacker *et al.*, "An ultra-low power InAs/AlSb HEMT W-band low-noise amplifier," in *IEEE MTT-S Int. Microw. Symp. Dig. (IMS)*, 2005, pp. 1-4.

[21] N. S. Killeen, D. P. Nguyen, A. N. Stameroff, A. Pham, and P. J. Hurst, "Design of a Wideband Bandpass Stacked HBT Distributed Amplifier in InP," in *IEEE Int. Symp. Circuits Syst. (ISCAS)*, 2018, pp. 1-5.

[22] N. Seiedhosseinzadeh and A. Nabavi, "Low noise amplifier linearization for near millimeter wave band applications," in *2nd Conf. on Millimeter-Wave and Terahertz Technologies (MMWaTT)*, 2012, pp. 48-51.

[23] X. W. Wu, C. Yu, H. L. Sun, and X. W. Zhu, "A millimeter wave digital pre-distortion platform for linearization of power amplifiers," in *IEEE Asia Pacific Microw. Conf. (APMC)*, 2017, pp. 1066-1068.

[24] R. Iommi, G. Macchiarella, A. Meazza, and M. Pagani, "Study of an active predistorter suitable for MMIC implementation," *IEEE Trans. Microw. Theory Techn.*, vol. 53, no. 3, pp. 874-880, 2005.

[25] Y. Youngoo and K. Bumman, "A new linear amplifier using low-frequency second-order intermodulation component feedforwarding," *IEEE Microw. Guided Wave Lett.*, vol. 9, no. 10, pp. 419-421, 1999.

[26] D. P. Nguyen, T. Nguyen, and A. V. Pham, "Development of a highly linear Ka-band power amplifier using second harmonic injection linearization," in *46th European Microw. Conf. (EuMC)*, 2016, pp. 835-838.

[27] A. Dani, M. Roberg, and Z. Popovic, "PA Efficiency and Linearity Enhancement Using External Harmonic Injection," *IEEE Trans. Microw. Theory Techn.*, vol. 60, no. 12, pp. 4097-4106, 2012.

[28] A. Dani, M. Roberg, and Z. Popovic, "Efficiency and linearity of power amplifiers with external harmonic injection," in *IEEE MTT-S Int. Microw. Symp. Dig. (IMS)*, 2012, pp. 1-3.

[29] C. S. Aitchison, M. Mbabele, M. R. Moazzam, D. Budimir, and F. Ali, "Improvement of third-order intermodulation product of RF and microwave amplifiers by injection," *IEEE Trans. Microw. Theory Techn.*, vol. 49, no. 6, pp. 1148-1154, 2001.

[30] Z. El-Khatib, L. MacEachern, and S. A. Mahmoud, "A fully-integrated linearized CMOS distributed amplifier based on Multi-Tanh principle for radio over fiber and ultra-wideband applications," in *Proc. IEEE Radio Wireless Symp.*, 2009, pp. 506-509.

[31] D. K. Paul and G. Parkinson, "A new approach for the linearization of a distributed amplifier," *Microw. Opt. Techn. Lett.*, vol. 46, no. 1, pp. 15-17, 2005.

[32] A. Jahanian and P. Heydari, "A CMOS distributed amplifier with active input balun using GBW and linearity enhancing techniques," in *Proc. IEEE Radio Freq. Integr. Circuits Symp. (RFIC)*, 2011, pp. 1-4.

[33] D. Webster, J. Scott, and D. Haigh, "Control of circuit distortion by the derivative superposition method [MMIC amplifier]," *IEEE Microw. Guided Wave Lett.*, vol. 6, no. 3, pp. 123-125, 1996.

[34] D. R. Webster and D. G. Haigh, "Low-distortion MMIC power amplifier using a new form of derivative superposition," *IEEE Trans. Microw. Theory Techn.*, vol. 49, no. 2, pp. 328-332, 2001.

[35] V. Aparin and L. E. Larson, "Modified derivative superposition method for linearizing FET low-noise amplifiers," *IEEE Trans. Microw. Theory Techn.*, vol. 53, no. 2, pp. 571-581, 2005.

[36] K. Tae Wook, K. Bonkee, and L. Kwyro, "Highly linear receiver front-end adopting MOSFET transconductance linearization by multiple gated transistors," *IEEE J. Solid-State Circuits*, vol. 39, no. 1, pp. 223-229, 2004.

[37] T. W. Kim, "A Common-Gate Amplifier With Transconductance Nonlinearity Cancellation and Its High-Frequency Analysis Using the Volterra Series," *IEEE Trans. Microw. Theory Techn.*, vol. 57, no. 6, pp. 1461-1469, 2009.

[38] C. Lu, A. V. H. Pham, M. Shaw, and C. Saint, "Linearization of CMOS Broadband Power Amplifiers Through Combined Multigated Transistors and Capacitance Compensation," *IEEE Trans. Microw. Theory Techn.*, vol. 55, no. 11, pp. 2320-2328, 2007.

[39] A. M. El-Gabaly, D. Stewart, and C. E. Saavedra, "2-W Broadband GaN Power-Amplifier RFIC Using the fT Doubling Technique and Digitally Assisted Distortion Cancellation," *IEEE Trans. Microw. Theory Techn.*, vol. 61, no. 1, pp. 525-532, 2013.

[40] H. Zhang and E. Sanchez-Sinencio, "Linearization Techniques for CMOS Low Noise Amplifiers: A Tutorial," *IEEE Trans. Circuits Syst. I: Regular Papers*, vol. 58, no. 1, pp. 22-36, 2011.

[41] Duy P. Nguyen, Nguyen L. K. Nguyen, Alexander N. Stameroff, Anh-Vu Pham, "A Highly Linear InP Distributed Amplifier Using Ultra-wideband

Intermodulation Feedforward Linearization," *in IEEE MTT-S Int. Microw. Symp. Dig. (IMS)*, June 2018, pp. 1-4.
[42] S. C. Cripps, *RF Power Amplifiers for Wireless Communications*. Artech House, 2006.
[43] G. Nikandish, R. B. Staszewski, and A. Zhu, "The (R)evolution of Distributed Amplifiers: From Vacuum Tubes to Modern CMOS and GaN ICs," *IEEE Microw. Magazine*, vol. 19, no. 4, pp. 66-83, 2018.
[44] D. P. Nguyen, T. Pham, and A. Pham, "A Ka-band asymmetrical stacked-FET MMIC Doherty power amplifier," in *Proc. IEEE Radio Freq. Integr. Circuits Symp. (RFIC)*, 2017, pp. 398-401.
[45] D. P. Nguyen, T. Pham, B. L. Pham, and A. V. Pham, "A High Efficiency High Power Density Harmonic-Tuned Ka Band Stacked-FET GaAs Power Amplifier," in *Proc. IEEE Compound Semiconductor Integr. Circuit Symp. (CSICS)*, 2016, pp. 1-4.
[46] D. P. Nguyen and A. V. Pham, "An Ultra Compact Watt-Level Ka-Band Stacked-FET Power Amplifier," *IEEE Microw. Wireless Compon. Lett.*, vol. 26, no. 7, pp. 516-518, 2016.
[47] D. P. Nguyen, T. Pham, and A. Pham, "A 28-GHz Symmetrical Doherty Power Amplifier Using Stacked-FET Cells," *IEEE Trans. Microw. Theory Techn.*, vol. 66, no. 6, pp. 2628-2637, 2018.
[48] B. Razavi, *RF Microelectronics (2nd Edition) (Prentice Hall Communications Engineering and Emerging Technologies Series)*. Prentice Hall Press, 2011, p. 960.
[49] D. Neamen, *Semiconductor Physics And Devices*. McGraw-Hill, Inc., 2003.
[50] M. D. Avino *et al.*, "A linearization technique for bipolar amplifiers based on derivative superposition," in *IEEE Bipolar/BiCMOS Circuits and Technology Meeting (BCTM)*, 2017, pp. 13-16.
[51] S. C. Cripps, *Advanced Techniques in RF Power Amplifier Design*. Artech House, 2002.
[52] K. Mæland, K. G. Kjelgård, and T. S. Lande, "CMOS distributed amplifiers for UWB radar," in *IEEE Int. Symp. Circuits Syst. (ISCAS)*, 2015, pp. 1298-1301.
[53] A. Arbabian and A. M. Niknejad, "Design of a CMOS Tapered Cascaded Multistage Distributed Amplifier," *IEEE Trans. Microw. Theory Techn.*, vol. 57, no. 4, pp. 938-947, 2009.

Duy P. Nguyen (M'17) received the B.S. degree (with highest honors) in electrical and electronics engineering from Vietnam National University, Ho Chi Minh City, Vietnam, in 2011, and the M.S. and Ph.D. degrees in electrical and computer engineering from the University of California, Davis, CA, USA, in 2014 and 2017, respectively. In 2017, he joined MACOM Technology Solutions Inc., Santa Clara, CA, USA, as a Senior Design Engineer where he designs optical linear drivers, and other RFICs and analog circuits. He has developed and designed a number of RFICs and MMICs in GaAs, GaN, InP, SiGe, and CMOS including power amplifiers, wideband distributed amplifiers, Doherty amplifiers, LNAs, T/R switches, phase shifters, fully integrated front-end modules, and linear drivers for optical modulators. He has authored and co-authored more than 20 patents, journals and conference papers. Dr. Nguyen was a recipient of Anil Jain Award for best Ph.D. dissertation from UC Davis, Spot Recognition Award from MACOM in 2018, and Vietnam Education Foundation (VEF) fellowship.

Nguyen L. K. Nguyen (S'16) received the B.E. degree (with highest Hons.) in Electrical Engineering and Information Technology from the Vietnamese German University, Binh Duong City, Vietnam, in 2016, and the M.S. degree in electrical engineering from the University of California at Davis, Davis, CA, USA, in 2019, where he is currently pursuing the Ph.D. degree. He has involved in designing RFICs in different technologies including InP, GaAs, and SiGe. His current research interest includes millimeter-wave power amplifiers, wideband amplifiers, and optical driver amplifiers. Mr. Nguyen was a recipient of the Vietnam Education Foundation Ph.D. Fellowship.

Alexander Stameroff (M'07) received the B.S., M.S., and PhD. degrees in electrical engineering from the University of California at Davis, CA, USA, in 2007, 2011, and 2013 respectively. During his graduate work he researched high efficiency GaAs and GaN power amplifiers for radar applications and was a recipient of the GAAN fellowship. He has been with Keysight Technologies since 2013 and designed both MMIC's and sub-systems. His research interests include hybrid and integrated circuit design at RF and millimeter-wave frequencies.

Anh-Vu Pham (SM'03) received the B.E.E. (with highest honors), M.S., and Ph.D. degrees in electrical engineering from the Georgia Institute of Technology, Atlanta, in 1995, 1997, and 1999, respectively. Anh-Vu joined the University of California at Davis in 2002 as an Assistant Professor and was promoted to full Professor in 2008. From 1999 to 2002, he was an Assistant Professor at Clemson University. Anh-Vu is conducting research in microwave and millimeter-wave integrated circuit design, power amplifiers, electronic packaging, sensors, energy harvesting, phased array antennas, and radar. His research has been supported by DARPA, National Science Foundation, Office of Naval Research, Air Force Research Laboratory and numerous companies. He has published ~200 peer-reviewed papers, several book chapters, and two books. Anh-Vu served as the Chair of IEEE Microwave Theory and Techniques (MTT) Technical Coordinate Committee on Microwave and Millimeter Packaging (2003-2006), and Chair of IEEE International Microwave Symposium Technical Committee on Power Amplifiers and Integrated Devices. He received the National Science Foundation CAREER Award in 2001 and the 2008 Outstanding Young Engineer Award from the IEEE Microwave Theory and Techniques Society. He was a Microwave Distinguished Lecturer of the IEEE MTT for the term 2010-2012. He was the Co-Chair of the Technical Program Committee for the IEEE International Microwave Symposium in San Francisco, 2016 and is the Co-Chair of the Technical Program Committee for the IEEE Asia Pacific Microwave Conference. Anh-Vu is currently a co-director of the Davis Millimeter Wave Research Center. In 1997, Anh-Vu co-founded RF Solutions, a fabless semiconductor company providing power amplifiers and RFICs for WiFi applications.

RF Solutions, Atlanta, GA, was acquired by Anadigics in 2003. In 2008, he co-founded and served as the CTO of Planarmag, Inc, West Sacramento, CA, which was acquired by TE Connectivity in 2010.